Conformational Relaxation in Hemoproteins: The Cytochrome P-450$_{cam}$ Case

Catherine Tetreau,* Martine Tourbez, and Daniel Lavalette*

Institut Curie, INSERM U350, Batiment 112, Centre Universitaire, 91405 Orsay, France

Received April 24, 2000; Revised Manuscript Received September 18, 2000

ABSTRACT: Photodissociation of (CO)P-450$_{cam}$(substrate) complexes was found to trigger a conformational relaxation process that interferes with ligand rebinding at temperatures as low as 140 K even though the protein conformational substates (CS[1]) remain frozen. To analyze the rebinding and relaxation kinetics, we developed a model that takes the distribution of relaxation rates explicitly into account and in which rebinding and relaxation rates are connected by a linear free energy relation. In all complexes heme relaxation occurs first and is probably faster than 100 ns even at 77 K. This is the only process found in substrate-free P-450$_{cam}$. Above 140 K and in the presence of a substrate, this initial, fast rebinding state (P*) progressively relaxes to another state (P°) in which rebinding is slower. The relaxation rate is independent of solvent rigidity and is governed by the protein's internal dynamics. Rebinding enthalpies in P* and P° as well as the enthalpy shift brought about by relaxation correlate with the substrate propensity to block access to the iron site. In P° the barrier is higher because the substrate is closer to the heme normal and exerts more steric repulsion for CO binding. The relaxation process implies the return of substrate and heme to their ligand-free positions in which access to the heme is reduced.

The principle according to which proteins assume a variety of energetically similar conformational substates (CS),[1] differing slightly in their activation enthalpy for simple ligand binding reactions, has proven extremely fruitful for explaining a vast body of experimental observations (*1*). It accounts for the nonexponential kinetics of phototriggered ligand rebinding reactions that are observed when proteins are embedded in a rigid environment at low temperature. In the absence of fluctuations between substates, as for instance in a rigid glass at low temperature, the kinetically heterogeneous protein ensemble is described by probability distributions $P(H)$ and $P(k)$ of the activation enthalpy H and of the reaction rate parameter k, respectively. The same concepts also explain exponential rebinding at physiological temperature and viscosity by kinetic averaging due to the rapid equilibrium fluctuations between CS. These concepts, first based on investigations of Mb, were later shown to be protein independent. They were first confirmed with the non-heme oxygen carrier hemerythrin (*2*). In more recent years azurin, an electron carrier copper protein (*3*), and several cytochromes P-450 (*4*) and NO synthase (*5*) were shown to display the same general behavior as Mb. It has been proposed that CS constitute a hierarchy (*6*, *7*), the lower members of which, CS^0, are a few "taxonomic" conformers. Each CS^0 is composed of a collection of conformational substates of higher order, CS^1, and so on (*7*−*10*).

Kinetic studies in rigid hydroorganic solvents are not sufficient to predict protein reactivity at high temperature and low viscosity. The temperature dependence of the enthalpy distribution is not known, and we can determine only the distribution $P(H,T_g)$ of the frozen CS ensemble at the solvent glass transition temperature T_g. Above about 200 K kinetic averaging may possibly lead to apparent preexponential factor and enthalpy values that are not necessarily simple averages of the distribution parameters (*11*). A quantitative understanding of the high-temperature reactivity is possible only if the underlying distribution is known. Moreover, since the conformation of a liganded protein differs from that of its unliganded counterpart, ligand photodissociation triggers relaxation processes that compete with rebinding (*12*). Because conformational relaxation is suppressed in a rigid medium, the low-temperature kinetics are representative of forced rebinding with a nonequilibrium protein conformation. Finally, concomitant with protein conformational changes and with the onset of protein fluctuations above T_g, the photodissociated ligand may explore new migration paths that are not accessible at lower temperature (*13*−*15*). Investigations of these various processes are therefore of prime importance to connect low-temperature concepts with the high-temperature regime in a quantitative fashion.

The current ideas about relaxation processes have been derived from studies of myoglobin, the prototype of hemoproteins. Above about 140 K new processes, not seen at lower temperature, interfere with CO rebinding (*16*−*19*). But despite the apparent simplicity of this protein, the structural origin of relaxation has long remained a matter of speculation.

The structure of myoglobin has been investigated using a variety of techniques such as X-ray diffraction (*20*−*22*),

* To whom correspondence should be addressed. Phone: 33-1-69 86 31 81. Fax: 33-1-69 07 53 27. E-mail: Daniel.Lavalette@curie.u-psud.fr; Catherine.Tetreau@curie.u-psud.fr.

[1] Abbreviations: Mb, myoglobin; sw Mb, sperm whale myoglobin; Hb, hemoglobin; P-450$_{cam}$(0), substrate-free cytochrome P-450$_{cam}$; P-450$_{cam}$(cam), camphor-bound cytochrome P-450$_{cam}$; P-450$_{cam}$(norcam), norcamphor-bound cytochrome P-450$_{cam}$; P-450$_{cam}$(adanone), adamantanone-bound cytochrome P-450$_{cam}$; P-450$_{cam}$(S), substrate-bound P-450$_{cam}$; MEM, maximum entropy method; CS, conformational substates; l.e., low enthalpy; h.e., high enthalpy.

10.1021/bi000920u CCC: $19.00
Published on Web 10/25/2000

neutron diffraction (*23*), and NMR (*24*). MbCO and deoxy-Mb differ in the heme geometry as well as in the position of some distal and proximal residues of the heme pocket. In MbCO, the heme is almost planar and the iron atom is in the heme plane. In deoxy-Mb, the heme is more domed and the iron atom is displaced toward the proximal side by 0.3−0.40 Å. Concomitant with the iron out-of-plane displacement, a slight change in the tilt and azimuthal orientations of the proximal histidine and a sliding motion of the F-helix are observed. Dissociation of carbon monoxide also induces significant movements in the distal His64. One water molecule that is hydrogen bonded to His64 in the distal heme pocket of deoxy-Mb is excluded from the pocket in the CO complex (*20*−*22*, *25*). Conformational relaxation following MbCO photolysis is thus a complex process implying proximal and distal structural rearrangements as well as entry of a water molecule into the distal cavity.

The idea that Mb relaxation was under the control of the proximal side and of the iron out-of-plane displacement has long prevailed (*16*, *26*−*28*). However, later spectroscopic evidence indicated that the kinetic coordinate governing the rebinding barrier cannot be the iron out-of-plane distance (*29*, *30*).

Numerous studies of myoglobin distal and proximal mutants have provided arguments favoring a distal control of relaxation (*31*−*33*). It was proposed that relaxation, as monitored by the spectral shifts of the Soret band and of the charge-transfer band III, results from a change in the electrostatic environment of the heme accompanying a reorganization of the solvent in the distal pocket (*33*).

The possible role of water in the relaxation process was suggested by the comparison of CO rebinding kinetics in a trehalose (*34*, *35*) and in a glycerol/water (*36*) glass by using the model of Agmon and Sastry (*28*) for fitting the kinetic data (*37*). Kleinert et al. (*38*) explained the slow reacting state observed in the CO rebinding with horse Mb by the entry into the distal cavity of the water molecule that is hydrogen bonded to His64 in the deoxy form, thus blocking the access of CO to the binding site.

However, recent reports on the crystal structure of the photolytic intermediates (*14*, *15*) tend to support an interpretation of the high-temperature geminate kinetics of Mb in terms of multiple docking sites of the CO ligand (*13*). The structural rearrangements that were successively proposed for Mb may occur in any hemoprotein, and any of them may eventually provide the rate-limiting step for relaxation. Since they may differ with proteins, relaxation may well constitute a case study.

Other hemoproteins, such as cytochromes P-450, share a number of kinetic properties with Mb though they perform enzymatic functions that are more complex than the oxygen storage and transport by Mb or Hb. Cytochromes P-450 are monooxygenases with a common active site consisting of a thiolate-coordinated iron(II) protoporphyrin IX. The function of cytochromes P-450 is to hydroxylate a substrate in a very stereospecific way. The substrate, which is bound in the heme pocket, has no direct interaction with the heme. We previously reported on the CO rebinding kinetics with cytochromes P-450$_{cam}$, P-450$_{SCC}$, and P-450$_{LM2}$ (*4*). As in other proteins, conformational substates (CS[1]) are at the origin of a distributed CO rebinding rate in a rigid environment at low temperature. However, in contrast to Mb, the enthalpy distribution $P(H)$ of cytochromes P-450 is often bimodal, consisting of a combination of a high- and a low-enthalpy distribution, $P(H)_{h.e.}$ and $P(H)_{l.e.}$. The structural origin of these subpopulations is not yet known. In P-450$_{cam}$ the subpopulations are approximately in a constant ratio, whereas in P-450$_{SCC}$ and P-450$_{LM2}$ they are in a thermal equilibrium, proving that some internal degree of freedom may still be mobile at a temperature as low as 77 K. Similar observations were recently reported with NO synthase (*5*). Because of this kinetic complexity, our first studies were limited to temperatures below 140 K where most protein movements are frozen so that additional complications due to relaxation processes could be avoided.

In cytochromes P-450 the amount of steric hindrance on the heme distal side, as well as the water occupancy of the pocket, can be modulated externally by varying the substrate. These advantages compensate for the greater structural and kinetic complexity of cytochromes P-450 compared to Mb. In the present work, we use this experimental flexibility to investigate kinetic relaxation in (CO)P-450$_{cam}$(substrate) complexes. The complexes investigated here fall into two distinct classes:

Class 1 complexes: (CO)Fe^{II}P-450$_{cam}$(0) and (CO)Fe^{II}P-450$_{cam}$(norcam). These hexacoordinated complexes contain either no substrate or the highly mobile norcamphor analogue. In the oxidized forms Fe^{III}P-450$_{cam}$(0) and Fe^{III}P-450$_{cam}$(norcam) a water molecule occupies the sixth coordination position of the iron atom.

Class 2 complexes: (CO)Fe^{II}P-450$_{cam}$(cam) and (CO)Fe^{II}P-450$_{cam}$(adanone). These are representative of complexes with rigidly immobilized substrates. The oxidized forms Fe^{III}P-450$_{cam}$(cam) and Fe^{III}P-450$_{cam}$(adanone) do not initially contain coordinated water.

It turns out that relaxation in cytochrome P-450$_{cam}$ differs in many ways from that reported for Mb. Relaxation kinetics are observed only with substrate-bound complexes above 140 K. In strong contrast to Mb, no relaxation kinetics were observed with the substrate-free P-450. We developed a new model to describe and to quantitatively evaluate relaxation kinetics. With this model, based on the use of rate spectra provided by an analysis using the maximum entropy method (MEM), the distribution of relaxation rates among CS is taken explicitly into account for the first time. Finally, the comparison of available crystal structures strongly suggests to assign the relaxation kinetics of P-450$_{cam}$ to a conformational relaxation involving a combined motion of both substrate and heme with respect to the protein environment. Such a process, which cannot occur in proteins with a simple ligand storage function such as Mb, might well be characteristic of more complex, substrate binding proteins.

MATERIALS AND METHODS

Materials. Recombinant cytochrome P-450$_{cam}$ (CYP101) (*39*) was a generous gift of Dr. C. Di Primo. The substrate-free protein was obtained by filtration through a Sephadex G-25 column. Camphor, norcamphor, and adamantanone were added to the substrate-free protein in a few microliters of an ethanolic stock solution (700 mM). A final substrate concentration of 10−30 mM was sufficient for complete saturation of the protein.

The required amount of cytochrome P-450$_{cam}$ was diluted with glycerol, buffer, and water. The final protein concentra-

tion was 10−15 μM in 50 mM Tris buffer, pH 7. The proportion of glycerol was either 64% (w/w) ($T_g \approx 160$ K, [CO] = 0. 62 mM) or 79% (w/w) ($T_g \approx 173$ K, [CO] = 0. 48 mM).

The ferrous (CO) complexes were prepared by passing a stream of CO above the protein solution submitted to gentle stirring and by adding a few microliters of a concentrated deaerated dithionite solution. CO binding was controlled by following the absorption change of the solution. The reduced complexes were obtained within a few minutes.

Methods. The methods used to collect and to process the data and to recover the rate parameters and enthalpy distributions have been described in detail in a previous work (*4*). They will be summarized only briefly.

(1) Data Collection. (CO)P-450$_{cam}$(substrate) solutions in gastight square cuvettes were cooled in a liquid nitrogen cryostat (Oxford Instruments DN704). Rebinding kinetics were recorded at 10 K intervals. The cooling rate was about 1 K/min, and the protein was allowed to equilibrate for a further 15 min once the desired temperature was stabilized. Photodissociation was achieved by the 10 ns pulse of the second harmonic (532 nm) of a Q-switched Nd:YAG laser (Quantel). Transient absorption changes, monitored at the peak of the Soret band of the hexacoordinated CO complex (446−448 nm), were recorded over 2 decades in amplitude and 6−7 decades in time using our fast kinetic spectrometer setup.

(2) Distribution of Rate Parameters and of Activation Enthalpy. At low temperature and high viscosity, ligand rebinding is nonexponential. The survival fraction $N(t)$ of unrecombined molecules is given by a weighted sum of exponentials (*1*):

$$N(t) = \int_0^\infty P(k) e^{-kt}\, dk \qquad (1)$$

in which $P(k)\, dk$ is the fraction of CS in the protein ensemble rebinding exponentially with rate k. The probability density function $P(k)$ provides an equivalent description of the rebinding kinetics but is considerably more powerful for analyzing complex processes.

In practice we obtain $P(\log k)$ from the observed kinetics $N(t)$ by Laplace inversion of eq 1 using the MEM with a set of logarithmically spaced k values. This amounts to solving

$$N(t) = \int_0^\infty P(\log k) e^{-kt}\, d(\log k) \qquad (2)$$

Equation 2 is mathematically equivalent to eq 1. The "rate spectrum" obtained by plotting $P(\log k)$ against $\log k$ is the most efficient presentation of complex kinetic data.

For an elementary kinetic process, the distribution of rates is caused by the distribution of the activation enthalpy $P(H,T)$ among CS, the preexponential factor A remaining sharp (*1*, *2*). Because of thermal equilibration among CS, the enthalpy distribution is, in principle, temperature dependent. However, below the solvent's glass transition temperature, T_g, interconversion among CS does not take place and the protein ensemble is frozen. The kinetics of an elementary process observed at any temperature below T_g are thus all derived from this unique, nonequilibrium and temperature-independent probability distribution of the activation enthalpy $P(H) = P(H,T_g)$. The validity of these basic assumptions has been repeatedly documented (*1*−*5*, *7*, *11*, *16*, *40*−*42*). $P(H)$ as well as the preexponential factor A was obtained from the linear plot of the barycenter of a series of $P(RT \ln k)$ at different temperatures (*4*). Note that even with a constant $P(H)$ the Arrhenius relation introduces a temperature dependence of $P(\log k)$ causing the latter to broaden upon lowering the temperature.

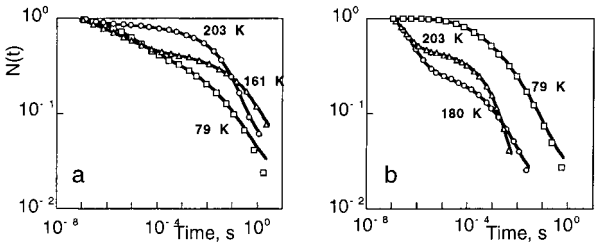

FIGURE 1: Kinetics of CO geminate rebinding with cytochrome P-450$_{cam}$(cam) (a) and P-450$_{cam}$(adanone) (b) between 79 and 203 K measured at the peak of the Soret band. For clarity, only three selected temperatures are shown. Symbols are data points. Lines are fits according to the MEM.

RESULTS

In cytochrome P-450$_{cam}$ as in Mb, the heme is a spectroscopic marker of choice for ligand binding studies. But conformational relaxation can be monitored only if structural changes are affecting the heme−ligand rebinding reaction or the heme spectral characteristics. Thus a succession of conformational states that do not significantly differ regarding the marker characteristics or the rebinding reaction is expected to escape detection and to appear as one kinetic state. In addition, conformational relaxation might continue once the marker has reached its final state or after rebinding is completed. Accordingly, the number of kinetically distinguishable states will always be equal to or smaller than the number of structural steps identifiable along the path of conformational relaxation. Experimental constraints also limit the observation of the marker to a time window. The earliest observable events are determined by the experimental time resolution of the equipment. We shall use, for short, P* and P° to denote the earliest and the latest observable protein conformations, respectively. P* and P° are defined relative to the experimental conditions and may vary according to the type of marker and experiment, whereas liganded and unliganded conformations are well-defined structural concepts. Experiments monitor relaxation from P* to P° but not necessarily the full relaxation from liganded to unliganded conformations. The distinction should always be kept in mind in order to avoid confusion.

(1) CO Rebinding with Cytochrome P-450$_{cam}$ Complexes. The kinetics of CO rebinding with the substrate-free cytochrome P-450$_{cam}$, as well as with its camphor-, adamantanone-, and norcamphor complexes, have been determined between 293 and 77 K. Not only do the nonexponential kinetics display a complex pattern with more than one process but the temperature dependence is reversed above 160 K. Displaying a series of such kinetics on a single graph becomes cumbersome because of the many curve crossings. For clarity, Figure 1 displays only a few representative examples of CO rebinding with the camphor- and adamantanone-bound complexes, showing the inverse temperature dependence observed above 160 K: the overall geminate rebinding becomes slower upon rising temperature.

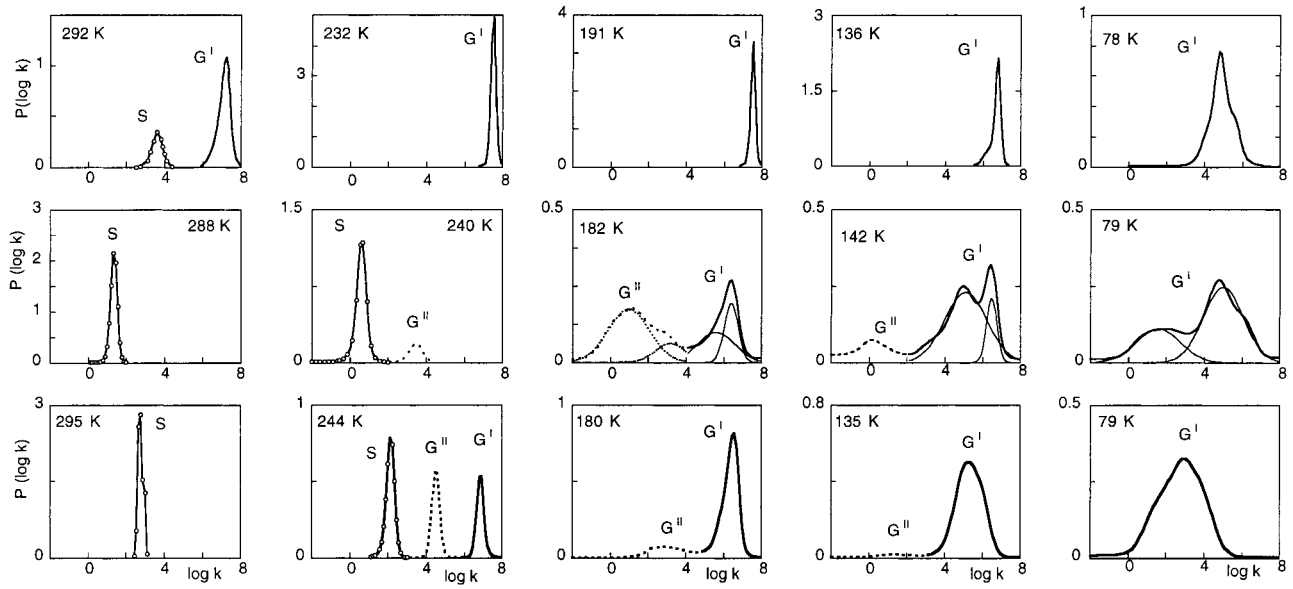

FIGURE 2: Normalized $P(\log k)$ rate spectra for CO rebinding with the class 1 complex P-450$_{cam}$(norcam) (top) and with class 2 complexes P-450$_{cam}$(cam) (middle) and P-450$_{cam}$(adanone) (bottom). S denotes the solvent process. G^I is attributed to geminate CO rebinding with the initial conformation of the protein P* and G^{II} to geminate CO rebinding with the final protein conformation P°. The thin lines and the dotted lines in the P-450$_{cam}$(cam) spectra (middle) correspond to the Gaussian decomposition of G^I and G^{II} as discussed in the text. The solvent was 64% glycerol/water (w/w) for adamantanone and norcam and 79% glycerol/water (w/w) for camphor. The data for P-450$_{cam}$(0) have been already published (*4*). They are essentially similar to those of P-450$_{cam}$(norcam).

The rate spectra of Figure 2 explain the complex pattern of the kinetics. Two or three well-separated groups of bands (respectively denoted by S, G^I, and G^{II}) are identified, indicating the presence of distinct processes. Their number and relative amplitudes depend on temperature as well as on the nature of the substrate. All processes are due to CO rebinding. The wavelength dependence of their initial amplitude follows the difference spectra between the hexacoordinated CO and pentacoordinated P-450 complexes (not shown). Bands G^I and G^{II} are independent of ligand concentration and correspond to geminate rebinding processes. Band S represents bimolecular rebinding from the solvent. It appears only above 200 K, and its peak rate coefficient is proportional to [CO].

Three temperature ranges must be distinguished:

(a) T < 130 K. At temperatures of at least 30 K below T_g, conformational substates do not interconvert. Each CS^1 reacts at its own rate, and $P(k)$ reflects the CS distribution. The simplest rebinding kinetics are observed at $T < 130$ K when most protein motions are frozen. In agreement with our previous findings, only one geminate rebinding process, G^I, was observed with all P-450$_{cam}$ complexes between 77 and 130 K. As reported previously, the rate distribution G^I of P-450$_{cam}$(cam) is bimodal (*4*). Such a kinetic heterogeneity is due to the coexistence of two different subsets of CS. In P-450$_{SCC}$ and P-450$_{LM2}$ the two subsets interconvert to some extent down to 77 K, whereas they remain approximately in a constant ratio in P-450$_{cam}$(cam). In this work, no clear evidence was found for CS subsets in P-450$_{cam}$(0), P-450$_{cam}$(norcam), and P-450$_{cam}$ (adanone) although we suspect that they actually exist. Their rate distributions are too close to be resolved, and one of the subsets probably dominates above about 100 K. In the temperature range of interest, process G^I can therefore be considered as unique in these complexes. Between 78 and 130−140 K the Arrhenius relation causes the rate spectra to progressively become narrower and to shift to faster rates. In P-450$_{cam}$(cam) the rates of the subpopulations tend to become closer.

(b) 130 K < T < 200 K. Above 140 K the evolution of the kinetic pattern markedly differs with substrate. Whereas the geminate process apparently remains unique in class 1, another slower process G^{II} appears in class 2 (dotted lines in Figure 2). Process G^{II} starts at $T \approx 135$ K and grows at the expense of G^I upon increasing the temperature. G^I and G^{II} are still distributed, and the two subsets of P-450$_{cam}$(cam) are apparent in both. Process G^{II} is responsible for the apparent slowing down and inverse temperature dependence of the overall kinetics in these complexes.

(c) T > 200 K. The appearance of bimolecular rebinding, process S, above about 200 K, provides evidence that equilibrium fluctuations have set in, allowing the escape of CO into the solvent. In class 2 complexes this process becomes predominant above 240 K, and the yield of CO escape, N_S, is equal to unity at room temperature. In contrast, the escape yield is much smaller in class 1, with an upper limit of 0.1−0.2 (a more accurate value cannot be given because geminate rebinding is very fast at these temperatures and, in part, escapes detection).

At the same temperature at which equilibrium fluctuations set in, kinetic averaging among CS is also observed. It is expected to affect slow rates first. Evidence for kinetic averaging is particularly apparent in the G^{II} rate distribution of P-450$_{cam}$(adanone) at 244 K (Figure 2, bottom) that, compared to the band at 180 K, is narrower than one would expect from the temperature increase alone. Note also that, at this temperature, the three processes are seen simultaneously with equivalent amplitudes. In P-450$_{cam}$(norcam) process G^{II} is observable as a kinetically averaged band of small amplitude in the very narrow temperature range 240−280 K (not shown in Figure 2).

(2) Relaxation in Distributed Systems: A New Approach. Process G^I is systematically observed with all complexes

Scheme 1: Relaxation Process within One CS

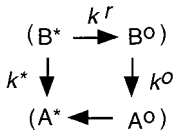

even in the lowest temperature range. It obviously corresponds to geminate CO rebinding with the initially observable P* conformation. We attribute band G^{II}, which only appears in the presence of a substrate above 140 K, to rebinding of protein molecules that have partially or totally relaxed to the unliganded P° conformation. In the Discussion section we shall establish a connection between the different substrate and heme positions and the liganded and unliganded P-450$_{cam}$ conformations, respectively. In our view this is the simplest explanation for the relaxation kinetics in P-450$_{cam}$, given the available kinetic and structural data. Consequently, we analyze the kinetics in terms of the irreversible parallel Scheme 1.

A most important feature is that protein relaxation is observed below T_g at temperatures at which CS^1 remain distributed, long before interconversion and kinetic averaging take place (Figure 2). This means that rebinding and relaxation remain confined within the individual CS^1. The internal motions at the origin of relaxation therefore belong to a higher tier of CS, presumably CS^2 (*6*), and each individual CS^1 must be characterized by particular rebinding and relaxation rates.

As a consequence, not only rebinding but relaxation as well are distributed processes, a fact that has not been previously considered explicitly. The usual approach in Mb studies was to postulate a time-dependent rebinding rate governed by a relaxation function of the activation enthalpy. By analogy with glasses, this function was assumed to be a stretched exponential. The use of rate spectra permits one to dispense with these assumptions and provides a more deductive approach of relaxation than fitting the survival curve using a global kinetic model that must be assumed a priori.

We first consider one single particular CS^1 with its ligand-bound (A) and dissociated (B) states. Observation begins when the protein is in the dissociated state B* of its P* conformation and ends in the bound state A° of its P° conformation. Since no CS^1 interconversion is taking place, dissociation, rebinding, and relaxation remain localized within that particular CS^1, as depicted in the kinetic Scheme 1. Observation in the Soret discriminates only between liganded and dissociated species. The states in parentheses in Scheme 1 are therefore spectroscopically indistinguishable. B* and B° are kinetically distinct, while A* and A° behave as one species. State A° is included for generality. It may have no independent physical existence, in which case a rebinding path would connect B° and A* directly. The distinction is without consequences for the following kinetic problem.

Below about 130 K, relaxation is slow and rebinding occurs uniquely from B* with rate k^*. At about 200 K, relaxation becomes so fast that rebinding takes place from the relaxed state B° with rate k^0. These limiting cases obviously provide no information about the relaxation process itself. Such information is obtained only at intermediate temperatures when rebinding from B* (process G^I) and from B° (process G^{II}) are simultaneously observed with respective rates $k^I = k^* + k^r$ and $k^{II} = k^0$.[2] A fraction $\varphi^* = k^*/k^I$ of the photodissociated ligand directly rebinds from B* as process G^I. Another fraction $\varphi^r = 1 - \varphi^*$ accumulates into B° from which subsequent rebinding takes place as process G^{II}. Because B* and B° are spectroscopically indistinguishable, the initial rise of B° exactly compensates the corresponding loss in B*. Finally, the total fraction of protein that has not rebound turns out to be

$$n(t) = \varphi^* e^{-k^I t} + \varphi^r e^{-k^0 t} \tag{3}$$

The rate spectrum thus consists of two lines centered at k^I and k^0, but whereas G^{II} always exhibits the true rate k^0 of relaxed rebinding, G^I corresponds to the composite rate k^I combining k^* and k^r. The relaxation rate and the rate of direct rebinding from B* are easily obtained from k^I and the amplitudes φ^* and φ^r by

$$k^r = \varphi^r k^I \tag{4}$$

and

$$k^* = \varphi^* k^I \tag{5}$$

The above results apply to each CS^1. For the ensemble of distributed CS^1 at $T < T_g$ the rate spectrum consists of two extended bands describing the distribution of G^I by $P_{exp}(\ln k^I)$ and that of G^{II} by $P_{exp}(\ln k^0)$. In terms of these experimental (MEM) distributions the survival kinetics are

$$N(t) = \int P_{exp}(\ln k^I) e^{-k^I t}\, d(\ln k^I) + \int P_{exp}(\ln k^0) e^{-k^0 t}\, d(\ln k^0) \tag{6}$$

The respective proportions Φ^* and Φ^r of G^I and G^{II} are equal to the integrals in eq 6 at $t = 0$. Unfortunately, the phenomenological eq 6 cannot be used in its present form for subsequent treatment because of the lack of a clearly identified independent variable. Although k^r and k^0 are distributed, their distribution functions are not known. Not only do they depend on the initial distribution of the B* substates but also they depend on which values of k^r and k^0 are connected to a given value of k^*.

The difficulty is best understood by deriving again the survival kinetics from eq 3, using k^* as the independent variable:

$$N(t) = \int P(\ln k^*) \varphi^* e^{-k^I t}\, d(\ln k^*) + \int P(\ln k^*) \varphi^r e^{-k^0 t}\, d(\ln k^*) \tag{7}$$

Note that the overall amplitudes of G^I and G^{II} are the average values of φ^* and φ^r expressed in terms of the elementary rates.

Thus:

$$\Phi^* = \int P(\ln k^*) \varphi^*\, d(\ln k^*) \tag{8}$$

and

[2] The approximation $k^0 \ll k^*, k^r$, suggested by experiment, has been used thoughout in the kinetic treatment.

$$\Phi^r = \int P(\ln k^*)\varphi^r \, d(\ln k^*) \quad (9)$$

The choice of k^* as the independent variable is forced upon us because $P(\ln k^*)$ directly reflects the initial distribution of CS[1] in P* when observation begins. It is the only distribution that can be unambiguously defined from measurement performed below T_g. But solving eq 7 in the general case requires functional relations connecting k^r and k^0 to the independent variable k^*. Such relations, which are not available a priori, must be provided by an additional physical model.

(3) Connection between k, k⁰, and kʳ: A Model.* Conformational substates are characterized by a set of activation enthalpies: H^*, H°, and H^r. All available evidence suggests that enthalpy varies smoothly among substates. Applying the linear approximation depicted in Figure 3, one obtains the following simple relations connecting H^r and H° with H^*:

$$H^r = aH^* + \Delta^r \quad (10)$$

and

$$H^\circ = bH^* + \Delta^\circ \quad (11)$$

Equations 10 and 11 allow for both a shift (Δ) and a change of width (a and b) of the enthalpy distributions $P(H^r)$ and $P(H^\circ)$ compared to $P(H^*)$. As a further consequence, the rate parameters are related to k^* by

$$k^r = \alpha k^{*a} \quad (12)$$

$$k^0 = \beta k^{*b} \quad (13)$$

Relations 12 and 13 between the rate parameters have the same form as that found using linear free energy relationships (LFER) for which many examples are known in physical chemistry. Such relationships are found in series of chemically closely related systems undergoing the same reaction. Since the conformational substates of a protein must be very closely related, the existence of a LFER-type relation is acceptable. The model now provides the desired functional connection relating all rates to k^*, and eq 7 can be, in principle, integrated.

In practice, unfortunately, one cannot expect four unknown parameters (a, b, α, and β) to be determined only from the available experimental data using eq 7. However, we may note that eqs 10−13 imply for the corresponding probability distributions:

$$P(H^*) = aP(H^r) = bP(H^\circ) \quad (14)$$

$$P(\ln k^*) = aP(\ln k^r) = bP(\ln k^0) \quad (15)$$

Therefore, the same CS[1] maximizes the three distributions expressed in terms of $P(H)$ or $P(\ln k)$. This simple conclusion[3] is an important one because we may now solve the problem for this particular CS by using the much simpler eqs 3−5, since $(\ln k^I)_{peak}$ and $(\ln k^0)_{peak}$ values of G^I and G^{II} can be clearly located. For this purpose, the corresponding φ^* and φ^r must be known. The peak probabilities are subject to some variability and can only be used as a crude approximation. The average values Φ^* and Φ^r obtained from the area of the distributions (eqs 8 and 9) are more reliable. But using Φ^* in place of φ^* to extract k^*_{peak} and k^r_{peak} from k^I_{peak} amounts to assuming that φ^* is constant among CS[1] and can be factored out in eqs 8 and 9. In other words, we have to assume that $k^r = \alpha k^*$ by setting $a = 1$ in eq 12. Both approaches gave similar results, but we preferred to use the Φ^* values because the scatter was less. This suggests that among the CS[1], the barrier for relaxation may be simply shifted by a constant amount compared to the barrier for rebinding, without changing the shape of the distributions. This is not unreasonable because k^* and k^r both originate from the same B* state. Such a constraint is not needed for k^0, and $P(H^\circ)$ is allowed to shift and to change shape compared to $P(H^*)$.

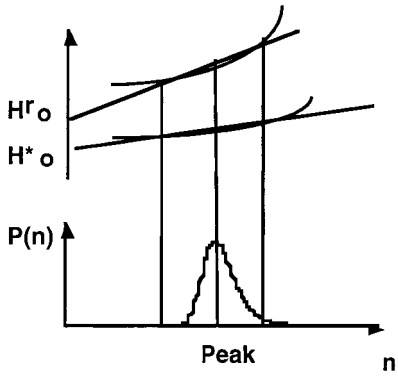

FIGURE 3: Conformational substates are sorted in increasing order of H^* values. The population distribution is sketched in the lower part of the figure. The correspondence between CS and enthalpy values H^* and H^r is assumed to be a smooth function (upper part of the figure). A straightforward linear interpolation leads to eqs 10 and 11.

(4) Enthalpy Distributions P(H) and P(H°) at T < T_g.* The derivation of $P(H,T_g)$ from the temperature evolution of the rate distribution below T_g (see Material and Methods section) applies to elementary processes only. For G^I, the treatment is valid in the range 77−140 K because relaxation is absent and $k^I = k^*$. It can be applied without restriction to G^{II} that always corresponds to the single rate k^0. However, G^{II} only appears above $T \approx 135$ K. Because of the smaller temperature range, the enthalpy distributions were determined with a lesser accuracy.

Another technical complication arises due to the bimodal rate distribution in P-450$_{cam}$(cam). This is solved by developing the enthalpy distribution according to

$$P(H) = \alpha_{h.e.}P(H)_{h.e.} + \alpha_{l.e.}P(H)_{l.e.} \quad (16)$$

in which $\alpha_{h.e.}$ and $\alpha_{l.e.}$ are the fractions of the high- and low-enthalpy subpopulations, respectively. Their temperature dependence can be neglected in P-450$_{cam}$(cam) (*4*).

A Gaussian decomposition of $P(\log k)$ yielded $P(H,T_g)_{h.e.}$ and $P(H,T_g)_{l.e.}$ that were independently normalized. This treatment was applied to both G^I and G^{II} processes. The preexponential factors and parameters characterizing enthalpy distributions are listed in Table 1 for the four P-450$_{cam}$ complexes. $P(H^*)$ and $P(H^\circ)$ distributions are shown in Figure 4.

(5) Relaxation Parameters. Peak relaxation rates and enthalpy distributions $P(H^r)$, calculated using our model, are

[3] Though in agreement with a certain common sense, the conclusion is actually by no means obvious. In particular, it is valid only for $P(\ln k)$ but not for $P(k)$.

Table 1: Preexponential Factor, A, Peak Enthalpy, H_p, and Width at Half-Maximum of the Enthalpy Distributions for CO Rebinding with Cytochrome P-450$_{cam}$(Substrate) Complexes[a]

	substrate	log A^* (s^{-1})	H^*_p (kJ/mol)	width (kJ/mol)	log $A°$ (s^{-1})	$H°_p$ (kJ/mol)	width (kJ/mol)
class 1	none	9.2 (0.1)	6.8 (0.2)	2.5 (0.3)			
	norcamphor	9.1 (0.1)	6.1 (0.2)	2.1 (0.3)	*7.9*	*8.4*	
class 2	adamantanone	8.9 (0.1)	9.1 (0.2)	4.2 (0.3)	7.3 (1.0)	15.1 (1.5)	4.7 (1.2)
	camphor (h.e.)	8.5 (0.6)	10.2 (1.2)	6.9 (1.8)	8.6 (1.8)	22.9 (5.5)	8.1 (1.5)
	camphor (l.e.)	8.0 (0.2)	4.1 (0.4)	4.2 (0.3)	4.9 (1.9)	15.3 (5.8)	3.4 (0.7)

[a] Solvent was 64% glycerol/water (w/w) except for camphor [79% glycerol/water (w/w)]. Values in parentheses are standard deviations of the least-squares fit to an Arrhenius equation. Because of the very small temperature interval in which relaxation is observed in norcamphor, the $H°$ parameters should be considered rather as estimates (italic).

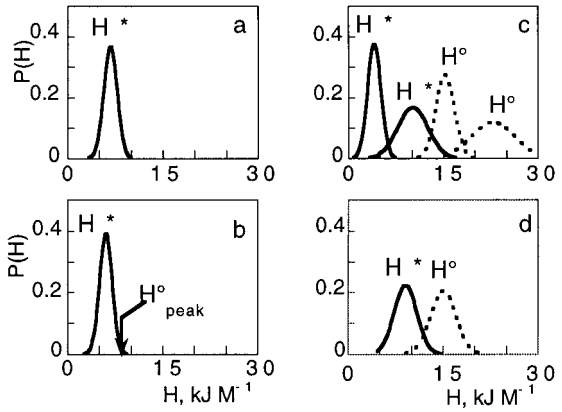

FIGURE 4: Normalized enthalpy distributions $P(H^*,T_g)$ (full lines) and $P(H°,T_g)$ (dotted lines) for CO rebinding with class 1 (left) and class 2 (right) complexes of cytochrome P-450$_{cam}$: (a) P-450$_{cam}$(0); (b) P-450$_{cam}$(norcam); (c) P-450$_{cam}$(cam); (d) P-450$_{cam}$(adanone). $P(H,T_g)$ were computed by merging all individual $P(H)$ obtained from measurements at $T < T_g$ and by fitting to a Gaussian. $P(H^*)$ was determined from measurements performed between 77 and 140 K. For $P(H°)$, the temperature range was limited because the relaxed band G^{II} was not observed below 135 K. In principle, measurements should be strictly restricted to temperatures below T_g ($T_g = 160-170$ K) where the CS enthalpy distributions are invariant. However, measurements were performed up to 180 K, and $P(H,180\ K)$ was not significantly different from the other distributions, indicating that any change of profile due to the change in the CS distribution or to a beginning of kinetic averaging was negligible. With norcamphor, process G^{II} was always kinetically averaged, so that no distribution profile can be given.

shown in Figures 5 and 6, respectively. The Arrhenius parameters are listed in Table 2.

Our measurements have been performed in buffer containing different amounts of glycerol [64% for P-450$_{cam}$(adanone) and 79% for P-450$_{cam}$(cam)]. For P-450$_{cam}$(cam), some measurements were also performed in 64% glycerol or in 60% ethylene glycol. At a given temperature, the viscosity of these solvents differs by at least 1 order of magnitude (*43*). The relaxation rate did not show any dependence on the solvent composition or viscosity. Below 220 K k^r_{peak} is faster by several orders of magnitude (Figure 5) than the solvent relaxation rate determined by specific heat spectroscopy (*38*). Moreover, the Arrhenius plot of the peak relaxation rates does not show any discontinuity at the glass transition temperature. All of these findings clearly indicate that protein relaxation is an internal process, decoupled from the bulk solvent and from the protein surface.

(6) Ligand Escape. Figure 2 reveals that bimolecular rebinding and, therefore, ligand escape from the protein are significant only above about 235−240 K. Another issue is whether CO escapes from P*, from P°, or from both states.

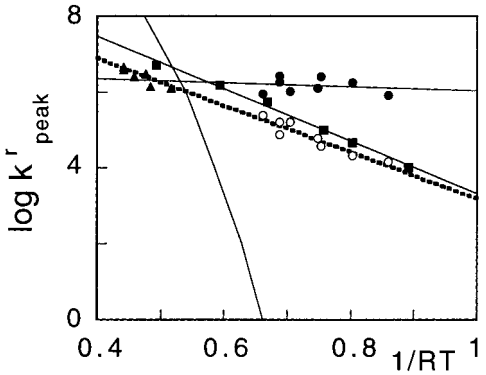

FIGURE 5: Arrhenius plot of the peak relaxation rate: P-450$_{cam}$(cam)$_{l.e.}$ population (filled circles) and P-450$_{cam}$(cam)$_{h.e.}$ population (open circles); P-450$_{cam}$(adanone) (squares); P-450$_{cam}$(norcam) (triangles). For P-450$_{cam}$(cam) the relaxation rates depend only to a minor extent on the manner in which h.e. and l.e. H^* are associated with h.e. and l.e. $H°$ distributions. No fit was performed with P-450$_{cam}$(norcam) because of the narrow temperature interval in which relaxation is observed. The solvent relaxation rate (79% glycerol/water) calculated from heat spectroscopy data (*38*) is shown for comparison (full line).

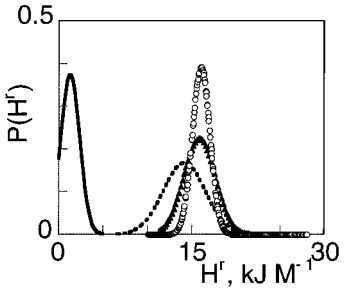

FIGURE 6: Enthalpy distributions $P(H^r)$ of the relaxation process calculated using the model described in the text: P-450$_{cam}$(cam)$_{l.e.}$ (full line) and P-450$_{cam}$(cam)$_{h.e.}$ (dotted line); P-450$_{cam}$(adanone) (triangles); P-450$_{cam}$(norcam) (circles). The distribution $P(H^r)$ of the P-450$_{cam}$(cam)$_{l.e.}$ subpopulation has been limited to positive values only.

To account for ligand escape from states B* and/or B°, two additional decay paths k^*_e and k^0_e must be added to the kinetic Scheme 1.

P-450$_{cam}$(adanone) at 244 K is the only case that can be solved completely because all three processes are simultaneously observed with significant amplitude (Table 3). At this temperature and above, we identify the kinetic averaged rate $\langle k \rangle$ with k_{peak}, the extrapolated peak value of the distributions.[4] $\langle k^* \rangle$ is first obtained by using eq 5, in which we put $\phi^* = N_I$ and $\langle k^I \rangle = \langle k^* \rangle + \langle k^r \rangle + \langle k^*_e \rangle$. Extrapolation from the low-temperature region yields k^r. It is found that $k^* + k^r$ almost exactly equal k^I, showing that k^*_e must be

Table 2: Arrhenius Parameters of the Peak Relaxation Rate k^r_{peak}[a]

	substrate	log A^r (s^{-1})	H^r_p (kJ/mol)
class 1	none		
	norcamphor	*9.7* (*0.8*)	*16.2* (*3.9*)
class 2	adamantanone	10.2 (0.2)	16.0 (0.7)
	camphor (h.e.)	9.4 (0.7)	14.1 (2.1)
	camphor (l.e.)	7.4 (0.9)	3.3 (2.8)

[a] Values in parentheses are standard deviations of the least-squares fit to the Arrhenius equation. Solvent was 64% glycerol/water except for camphor (79% glycerol/water).

Table 3: Kinetically Averaged Rate Parameters (s^{-1}) for CO Rebinding with P-450_{cam}(Adanone) in 64% Glycerol in the High-Temperature Region ($T > 230$ K)[a]

	293 K/ 15 cP	244 K/ 320 cP		293 K/ 15 cP	244 K/ 320 cP
N_S	1	0.43	$\langle k^*_{esc}\rangle$	$\geq 10^9$	$\ll 10^6$
N_I	0	0.27	φ^r	0	0.73
N_{II}	0	0.30	k^{II}		8.8×10^4
k^I		8×10^6	$\langle k_0\rangle$		3.6×10^4
$\langle k^*\rangle$	$[2 \times 10^7]$	2.2×10^6	$\langle k^0_{esc}\rangle$		5.2×10^4
$\langle k^r\rangle$	$[2 \times 10^7]$	$[6 \times 10^6]$			

[a] N_S, N_I, and N_{II} are the amplitudes of processes S, G^I, and G^{II}, respectively. The values in brackets were extrapolated from the low-temperature region (Table 1).

negligible. The relaxation yield $\phi^r = (1 - N^I)$ amounts to 0.73. For the amplitude of relaxed rebinding we have $N_{II} = \phi^r\langle k^0\rangle/\langle k^{II}\rangle$, in which now $\langle k^{II}\rangle = \langle k^0\rangle + \langle k^0_e\rangle$, giving the values listed in Table 3. It turns out that CO escape at 244 K takes place only in P° with rate $\langle k^0_e\rangle = 5.2 \times 10^4\ s^{-1}$.

At 293 K only the solvent process is observed ($N_S = 1$). Since $N_I = \langle k^*\rangle/(\langle k^*_e\rangle + \langle k^r\rangle + \langle k^*\rangle)$ is zero (or less than a few percent), an extrapolation of k^* and k^r from the low-temperature region yields the estimate $k^*_e \approx 10^9\ s^{-1}$. At 293 K the ligand escapes in P* before relaxation takes place. We conclude that CO escape may in principle occur in either of the protein states. The other complexes cannot be solved as easily because complete data are not available. They are discussed later.

DISCUSSION

Comparison of Relaxation Models. The kinetics of ligand rebinding with cytochrome P-450 exhibit a complexity comparable to that reported long ago for Mb (*1*, *16*, *43*). The main features are (i) the existence of distributed barriers that are best observed at temperatures well below T_g (Figure 2) and (ii) an inverse temperature effect characterized by a slowing down of the kinetics upon increasing the temperature above 140−180 K (Figure 1). Historically, the Mb kinetics below T_g were treated by postulating some parametrizable function (exponential, Gaussian, or gamma) to describe the enthalpy distributions. The parameters were then optimized to reproduce the experimental kinetics using least-squares fits (*1*, *7*, *12*, *42*). The problem of the inverse temperature effect is of a different nature. In Mb it was first addressed by assuming that the ligand has to overcome a series of energy barriers disposed sequentially along the reaction coordinate (*1*). The number of barriers was determined empirically (sometimes up to four were found to be necessary) until the fit to the data was satisfactory. But whereas a combination of several sequential barriers with different temperature dependences constitutes a model with sufficient complexity to fit kinetic data, the reality of the postulated intermediate states cannot be proven by kinetic considerations alone. The multiple barrier model was later rejected in favor of a relaxation model in which the rebinding rate was time dependent and the enthalpy barrier was assumed to shift in time according to a stretched exponential law (*16*, *38*). However, recent evidence of multiple CO docking sites in Mb again emphasizes the role of sequential barriers in the high-temperature kinetics of MbCO (*13*−*15*).

The present MEM approach of cytochromes P-450 kinetics is basically different and dispense with unnecessary assumptions. The rate spectra are not simulated data. They represent, in the rate domain, an alternative and equivalent description of the data as the kinetics in the time domain. The advantage of rate spectra is that pertinent information is retrieved more easily. We do not postulate a barrier number, but we use the rate spectra in a simple deductive manner. Figure 2 immediately indicates [notwithstanding the more complicated case of P-450_{cam}(cam)] that one unique distributed barrier accounts for the kinetics below 140 K but that two distributed barriers are observed above this temperature with class II compounds. This unambiguously determines the number of barriers.

The model we use to analyze the temperature evolution of the rate spectra also differs from those previously applied to relaxation studies in Mb. Since rebinding barriers are distributed, a consistent description of the relaxation process implies that the distribution of relaxation rates should be considered as well.

The connection of the present model (eqs 3, 6, 12, and 13) with the time-dependent rebinding rate model previously used in Mb studies can be understood by writing the derivative of eq 3 in the form $dn/dt = k(t)n$, yielding an apparent time-dependent rate parameter:

$$k(t) = \left(\frac{\varphi^* k^I e^{-k^I t} + \varphi^r k^0 e^{-k^0 t}}{\varphi^* e^{-k^I t} + \varphi^r e^{-k^0 t}}\right) \qquad (17)$$

The equivalence thus established between models is purely formal. Similarly to many other physical problems, the time dependence appears because the problem was not stated in terms of the system "eigenstates". In the present problem these states are P* and P°. In other words, one particular molecule rebinds only either with rate k^* or with rate k^0 after experiencing a transition with rate k^r. The choice of a stretched exponential to describe the enthalpy change accounting for $k(t)$ was probably a convenient one for performing least-squares fittings of the kinetics. But simulations using eq 17 with realistic values of the rate parameters showed that acceptable fits could only be obtained with particular sets of parameters for the stretched exponential. In addition, these models used one unique "enthalpy relaxation function" for all substates so that the distribution of relaxation rates was taken into account only indirectly.

A description of the relaxation kinetics in terms of distributed elementary processes k^*, k^r, and k^0 is simpler and more consistent. Equations 6 and 7 show that the problem

[4] Upon rising temperature, $P(\log k)$ always narrows, even at constant $P(H)$, so that $\langle k\rangle$ and k_{peak} may become quite close for a narrow distribution.

can be solved only if some functional relation connects the rate parameters within one CS[1]. We use eqs 12 and 13 that are closely related to linear free energy relationships. Though other choices might be possible, we believe that this is the most natural assumption.

Another issue is whether the two barriers are arranged in parallel as we have assumed in Scheme 1 or disposed sequentially as in the alternative Scheme 2.

Scheme 2: Sequential Model

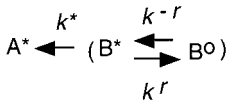

The kinetic equations have the same form as eq 3, and the rate parameters k^* and k^r are still given by eqs 4 and 5 using the same observables.[5] Schemes 1 and 2 only differ in the rate of the slower process. For the sequential scheme:

$$k^{II} = \frac{k^* k^{-r}}{k^I} = \Phi^I k^{-r} \qquad (18)$$

Whereas $k^{II} = k^0$ in the parallel relaxation scheme, it becomes a composite rate in the sequential scheme and should, in principle, display a non-Arrhenius behavior. In practice, the curvature of the Arrhenius plot would become significant only for $\Phi^I \ll 0.5$. Unfortunately, the experimental test is not possible since ligand escape sets in well before a high enough temperature can be reached to decrease Φ^I noticeably. Thus, in a sequential scheme, the relation $k^{II} \approx k^{-r}$ is approximately valid over the whole temperature range. Obviously, the physical interpretation of the states B* and B° and of the rate parameters k^r and k^{-r} will differ with the postulated scheme, but as expected, kinetics alone are not sufficient to support unambiguously one or the other. Note that a sequential scheme does not describe an irreversible relaxation process, because the rebinding state is always B*. Scheme 2 would apply if, for instance, the ligand became trapped in a long-lived docking site similar to the proximal Xe(1) site reported in Mb (*13*−*15*). The access of CO to this site probably requires collective motions of parts of the protein that become effective near 180 K and also promote ligand escape. Whether such sites exist in P-450$_{cam}$ is presently unknown. Process G^{II} starts at significantly lower temperature, and such fluctuations are not likely to be entirely decoupled from the solvent in contradiction with the data shown in Figure 5. Though independent spectroscopic evidence for conformational relaxation is not available yet for P-450, we shall see shortly that structural differences between liganded and unliganded forms are significant and clearly documented; it is therefore natural to look for their kinetic signature in terms of the irreversible parallel reaction Scheme 1 rather than in terms of sequential barriers. We consequently proceed to the specific discussion of the P-450 results in terms of the relaxation Scheme 1.

[5] Kinetic Scheme 2 has been used in so many contexts that we may dispense with a detailed derivation. Note that the distributed relaxation approach described in Results sections 2 and 3 applies to the sequential scheme as well. Below about 200 K, k^0 should be replaced by k^{-r} in eqs 6−13.

Depending on substrate and temperature, geminate CO rebinding with P-450$_{cam}$(S) complexes involves one or two processes. In class 2 complexes no geminate rebinding can be seen at room temperature ($N_S \approx 1$). At low temperature two processes are observed: process G^I occurs first and is fast, but the system also relaxes, on the same time scale, to a new conformation in which rebinding follows the much slower process G^{II}. In class 1 complexes at room temperature N_S is small, and the geminate rebinding rate is fast, though still observable. Over the whole temperature range only process G^I is observed in P-450$_{cam}$(0), whereas in P-450$_{cam}$(norcam) process G^{II} appears at higher temperature, but only transiently, within a narrow interval and with a small amplitude.

Below T_g, rebinding and relaxation are distributed processes, and CS[1] rebind and relax independently of each other. Using a MEM analysis and a relatively simple model taking the distribution of relaxation rates explicitly into account, we were able to characterize $P(H^*)$ for all complexes as well as $P(H^\circ)$ and $P(H^r)$ for substrate-bound complexes. The main features of CO rebinding and protein relaxation can now be summarized as follows.

Relaxation reduces the CO geminate rebinding rate by several orders of magnitude mainly because the enthalpy barrier increases in a way that is more or less pronounced according to the nature of the substrate (Figure 4 and Table 1). The peak relaxation rate k^r_{peak} varies continuously with temperature. Below 220 K it always exceeds the solvent dynamic relaxation rate by several orders of magnitude, and no discontinuity is observed near the glass transition temperature T_g (Figure 5). Therefore, relaxation is not coupled to the bulk or surface solvent and must be driven by the protein's internal dynamics. Relaxation is observed only in the presence of a substrate, and its rate and enthalpy appear surprisingly similar among substrates ($H^r \approx 14-16$ kJ/mol) (Figure 6).

The rebinding enthalpy distribution shifts by an amount $\Delta H = H^\circ - H^*$ that increases in the order norcamphor (≈2 kJ/mol) < adamantanone (6 kJ/mol) < camphor$_{h.e.}$ (12.7 kJ/mol) ≈ camphor$_{l.e.}$ (11.2 kJ/mol).

The rebinding enthalpies follow the same ascending order: for H^*, no substrate (6.8 kJ/mol) ≈ norcamphor (6.1 kJ/mol) < adamantanone (9.1 kJ/mol) ≤ camphor$_{h.e.}$ (10.2 kJ/mol); for H°, norcamphor (8.4 kJ/mol) < adamantanone (15.1 kJ/mol) < camphor$_{h.e.}$ (22.9 kJ/mol). As seen in Tables 1 and 2, the camphor$_{l.e.}$ subpopulation constitutes an exception as reflected in H^*, H^r, and H°.

Relaxation sets in at very low temperature (≈130−140 K) in class 2 complexes, but G^{II} is seen only above 240 K in P-450$_{cam}$(norcam) despite a similar relaxation rate. This is a simple consequence of the large rebinding rate k^* of P-450$_{cam}$(norcam): the crossing of the Arrhenius plots of k^* and k^r occurs at a higher temperature, and k^r begins to compete efficiently with k^* only above about 240 K.

In hemoproteins, three main differences between liganded and unliganded conformations may be distinguished: (i) changes in the heme geometry, in the position of the Fe(II) atom with respect to the porphyrin plane, and, by extension, in the position of the proximal (histidine or thiolate) ligand; (ii) changes in the distal heme pocket involving side chain displacements and rotations; (iii) in addition, multiple docking sites, such as the xenon sites in Mb, may be explored

by the ligand; with cytochromes P-450 whose catalytic function requires the presence of a substrate and of a variable number of water molecules in the heme pocket, attention should be paid to changes in the substrate position and to the pocket water occupancy; (iv) changes in tertiary structure such as helix and loop displacements. These are comparatively slow processes that may be expected to affect the heme only to a minimal extent, if any, as they often concern protein regions far removed from the heme. They probably escape detection.

Heme Relaxation and Assignment of G^{I}*. (1) Heme Conformational Relaxation.* Crystallographic studies of photodissociated MbCO performed at low temperature have yielded controversial results regarding heme relaxation. Schlichting et al. (*44*) and Hartmann et al. (*45*) concluded that the displacement of the iron and the doming of the heme were almost complete in the Mb* structure after photolysis at 20−36 K. In contrast, Teng et al. (*46*) reported that relaxation of the heme was greatly reduced at $T < 160$ K with no residue shifting by more than 0. 15 Å and with only a small displacement of the iron atom.

Despite the number of crystal structures available, our knowledge about cytochromes P-450 complexes is mainly limited to the oxidized (Fe^{III}) forms that do not bind CO. The single known structure of a carboxy species is that of (CO)Fe^{II}P-450_{cam}(cam) (*47*). The crystal structure of the pentacoordinated Fe^{II}P-450_{cam}(cam) species has become available only quite recently (*48*). It is reported to be essentially the same as that of Fe^{III}P-450_{cam}(cam) (*49*, *50*). A comparison of these data indicates that, upon reduction and CO binding, the heme iron atom moves closer to the heme plane, the S−Fe bond lengthens from 2.2 to 2.4 Å, and the camphor substrate is displaced away from the CO molecule by about 0.8 Å (*47*). Finally, the heme changes are quite comparable to those found in myoglobin. Thus, if heme relaxation were taking place in the Mb crystal at 40 K, one may reasonably expect heme relaxation to occur also at 77 K in P-450_{cam}.

(2) Assignment of G^{I}*.* The fast process G^{I} is seen in all complexes below T_g, but at room temperature fast and exponential geminate recombinations are observed with class 1 complexes only. In P-450_{cam}(0) the kinetic average at 293 K agrees within a factor of 2 with the extrapolation of G^{I} from the low-temperature region, suggesting that the same process is seen throughout the whole temperature range 77−293 K. The absence of relaxation and of G^{II} in substrate-free P-450_{cam}(0) argues against an explanation of G^{II} in terms of movements of the iron out of the heme plane as was originally believed for Mb (*16*, *26*−*28*). On the other hand, the heme has certainly relaxed at 293 K. Out-of-plane displacement of the iron, heme doming, and small changes in the positions of the amino acids localized at a close proximity of the active center are expected to be very rapid and fall in the subnanosecond domain at room temperature (*30*).

Experimental kinetic data therefore show no evidence of any process that could possibly correspond to heme relaxation on the time scale explored in this work. Thus, when observation starts about 10−20 ns after photolysis, CO rebinds in P* where the heme (but not necessarily the distal pocket or the tertiary structure) has already relaxed to its deoxy conformation. Because of the continuity of *k**, heme relaxation probably remains faster than 100 ns even at the lowest temperatures, in agreement with the observations of Schlichting et al. (*44*) and of Hartmann et al. (*45*).

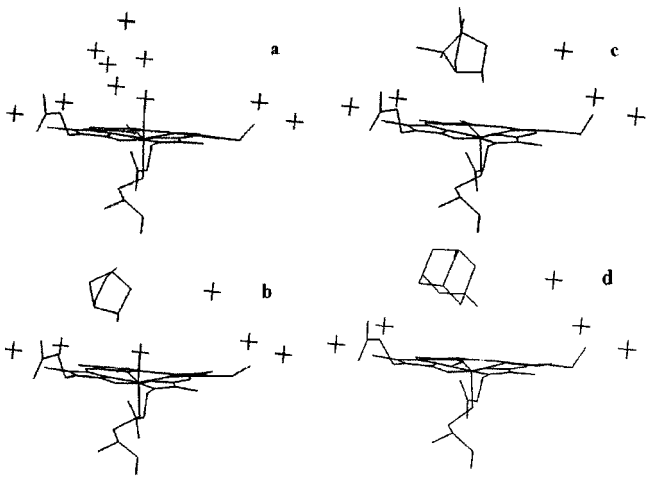

FIGURE 7: Heme pocket of (a) Fe^{III}P-450_{cam}(0), (b) Fe^{III}P-450_{cam}(norcam), (c) Fe^{III}P-450_{cam}(cam), and (d) Fe^{III}P-450_{cam}(adanone) according to their crystal structures (*50*, *52*, *60*). These views were obtained with the Insight II (MSI, San Diego) software and the respective PDB entries: 1PHC, 7CPP, 2CPP, and 5CPP. Crosses denote water molecules that are within 11 Å of the Fe atom. The views are 20° clockwise from the direction of pyrrole D (front) and B (rear) nitrogens.

Pocket Reorganization and Relaxation Mechanism. In all substrate-bound complexes the additional process G^{II} progressively replaces G^{I} above 140 K. To discuss the possible origin of G^{II}, we first review the present knowledge on the organization and occupancy of the distal pocket in P-450_{cam} complexes (Figure 7).

The volume of the distal cavity of Fe^{III}P-450_{cam}(0) is large enough to accommodate up to 10 water molecules (*51*). Six water molecules were identified in the crystal structure (*52*) (Figure 7a). One of them provides the sixth axial ligand of Fe^{III}, resulting in a low-spin state characterized by a Soret absorption band maximum at 418 nm. The six water molecules (including the aqua ligand) are expelled from the distal cavity upon binding camphor (*49*, *50*) (Figure 7c). The pentacoordinated state of Fe^{III}P-450_{cam}(cam) is high spin and has a maximum of absorption at 392 nm. Conversely, six water molecules bind when camphor is expelled from the protein (*53*). The spin state is an indicator of the water accessibility to the Fe^{III} atom and of the degree of solvation of the pocket (*54*−*58*). Access of water molecules to the pocket is largely determined by the substrate mobility that depends on the proper hydrophobic contacts of its C-10 methyl groups with the protein residues rather than on its size and hydrogen bonding of the keto group with Tyr96 (*57*, *58*). In the crystal structures of Fe^{III}P-450_{cam}(substrate) complexes with substrates that are rigidly maintained both by hydrophobic contacts and by hydrogen bonding with Tyr96 such as 1*R*- or 1*S*-camphor (*49*, *53*, *59*) or adamantanone (*60*), water molecules are absent and the iron is in the high-spin state (Figure 7c,d). In contrast, substrates such as norcamphor, lacking the methyl group contacts with the protein, have a lower high-spin content and contain one water molecule assigned by crystallography (*60*) (Figure 7b). The presence of one ordered water molecule and likely of disordered solvent has also been reported for camphane,

adamantane, and thiocamphor that are less firmly held than camphor (*61*). As shown in Figure 7, water coordination is correlated with steric crowding of the heme normal by the substrate. The favored perpendicular geometry of CO would hardly be possible without substrate rearrangement in class 2 complexes. It is expected to be easier in P-450$_{cam}$(norcam) because the heme normal is less encumbered, as confirmed by the presence of the aquo coordinate in the Fe^{III} form. This coordinated water is very likely to be removed from the iron in the reduced form since water binding to a reduced heme has been observed only in rather exceptional circumstances (*62*, *63*).

Kinetic and structural investigations of sterically encumbered heme models have revealed that the perpendicular Fe−C−O geometry is considerably more resistant to steric hindrance than was originally believed. In crowded systems, the destabilizing energy was found to be essentially relieved by distortions of the steric obstacle or even of the heme itself, so that the perpendicular Fe−CO geometry is preserved as much as possible (*64*, *65*). It is therefore not surprising that changes of the heme pocket organization also occur upon CO binding with P-450$_{cam}$(cam).

We have performed a comparison of heme and substrate positions in Fe^{III}P-450$_{cam}$(cam) (*50*) and (CO)Fe^{II}P-450$_{cam}$(cam) (*47*) by superposing the protein backbone. RMSD for the backbone superposition was 0.133 Å. Assuming that reduction of the iron does not affect much the protein structure (*48*), two motions are found to alter the relative position of heme and substrate upon binding CO. The first one, which does not seem to have been noticed before, is a sliding motion by 0.2 Å of the heme in its plane perpendicular to the propionate direction. The dominant substrate displacement is 0.5 Å toward the propionates with a smaller contribution of 0.15 Å opposite to the heme motion. Camphor is also displaced by 0.11 Å farther away from the heme plane. In these motions, the camphor oxygen atom remains hydrogen bonded to Tyr96 with a constant bond length. The motion of the substrate may thus be pictured as that of a pendulum swinging around Tyr96. Though (CO)Fe^{II}P-450$_{cam}$(cam) is the only carbonylated complex with a known crystal structure, the other substrates, which are even less firmly bound than camphor, are very likely to experience a similar displacement upon binding CO.

The structure of Fe^{III}P-450$_{cam}$ complexes (Figure 7) together with the substrate−heme motions provides a rational explanation for the activation enthalpy ordering of the complexes as well as a probable mechanism for the relaxation process in cytochrome P-450$_{cam}$. The CO binding enthalpies follow the ordering expected from the apparent steric hindrance of the substrate: no substrate < norcamphor < adamantanone ≈ camphor. Although we cannot distinguish clearly between adamantanone and camphor by simply considering Figure 7, the ligand obviously does. The highest enthalpies are found in P° because the destabilizing effect upon the transition state is the largest in the relaxed substrate position that is closer to the heme normal. In the CO-bound state, substrate and heme have moved apart. Norcamphor now exerts little steric hindrance, and P-450$_{cam}$(norcam) reacts in P* almost exactly like substrate-free P-450$_{cam}$ (Table 1). Removal of steric hindrance seems to be incomplete with camphor and adamantanone. Although they now react much faster in P*, the H^* enthalpies still keep the same order as found in P°. Crystal structures of (CO)Fe^{II}P-450$_{cam}$(norcam) and (CO)Fe^{II}P-450$_{cam}$(adanone) would be very valuable for confirming this picture.

Since no other significant difference was found in the protein structure, the reverse motion of substrate and heme, restoring their ligand-free position after photodissociation of CO, must provide the relaxation mechanism. Because these are local motions that take place in the protein interior, they are not submitted to external friction, in agreement with the finding that relaxation rate does not depend on the external viscosity (Figure 5). Since they imply relatively small groups, they constitute a degree of freedom that may still be mobile down to low temperature.

The important feature is that relaxation proceeds at a rate that does not seem to be much affected by the nature of the substrate (again excluding the particular case of camphor$_{l.e.}$). As a crude analogy, one might imagine the substrate motion as a rotation around the Tyr96 OH group. In a harmonic potential, the "frequency" of the free return to equilibrium after removal of CO would be independent of the initial amplitude, i.e., of the substrate-dependent displacement brought about by the CO ligand. The presence of a different number of methyl groups interacting with the protein makes this picture obviously a very rough one. Another possibility is that the substrate motion is fast and that the heme motion might be the rate-limiting kinetic step of the relaxation process. Unfortunately, the time scale of these motions is beyond the present possibilities of molecular dynamics simulations.

Role of Water. The catalytic pathway of P-450$_{cam}$ requires the presence of water. The surrounding of the heme pocket is initially highly hydrated, as shown in Figure 7. An alternative relaxation mechanism, implying entry of water into the pocket and comparable to that recently suggested for Mb (*38*), might be imagined. Although coordination of water to the Fe^{II} heme, followed by a slow, k_{off}-limited, exchange with CO, would cause a slowing down of rebinding as well, no evidence for water coordination to the reduced heme was found. Our kinetics never showed an indication of a spectroscopically distinct transient state, particularly at the sensitive wavelengths near the isosbestic point of pentacoordinated and CO-hexacoordinated P-450$_{cam}$. The recent release of the crystal structure of the pentacoordinated Fe^{II}P-450$_{cam}$(cam) species confirms the absence of water near the vacant sixth position (*48*). Thus, direct coordination of water to the heme or even reduced access due to the presence of water in the close vicinity of the heme may be excluded as an alternative cause for G^{II}.

Substrate and heme motions do not seem sufficient, however, to provide an explanation for the striking difference in the ligand escape rate between class 1 and class 2 complexes. For the sake of generality we have distinguished between k^*_e and k^0_e, but this distinction may not be physically necessary. One unique common escape rate, k_e, resulting from substrate-independent protein fluctuations, would explain the data as well. Ligand escape appears to take place in P* or in P° simply according to the relative values of k_e and k^*. Experimental evidence indicates that ligand escape is generally governed by structural fluctuations at the protein surface and is thus sensitive not only to temperature but also to the external viscosity (*2*, *43*, *66*). The latter is known to vary quite rapidly with temperature (the apparent activation

energy is $E_a \approx 38$ kJ/mol for the 64% glycerol mixture). The considerable temperature dependence of the CO escape rate in P-450$_{cam}$(adanone) is in accord with these views.

In P-450$_{cam}$(0)[6] and P-450$_{cam}$(norcam) k^* is about 10^8 s^{-1} at 293 K. Process G^{II} is not observed with the latter complex at this temperature, but k^r and k^0 extrapolate to about 8×10^6 s^{-1} and 3×10^6 s^{-1}, respectively. If k^*_e were fluctuation limited as suggested for P-450$_{cam}$ (adanone), its high rate ($\approx 10^9$ s^{-1}) would cause escape to be complete and process G^I would not be observed. Thus, in these complexes, the escape rate is smaller than expected for the fluctuation-driven process. We observe that a value of $k^*_e \approx 10^7$ s^{-1} would account for the data quite well: In P* about 88% of the CO molecules would rebind and nearly 9% would escape. The remaining 3% would relax but immediately escape because $k^0 \ll k_e$, thus explaining that process G^{II} has disappeared at this temperature.

The proportion of the subpopulations of P-450$_{cam}$(cam) are not known above T_g, and rates cannot be calculated. However, escape in P-450$_{cam}$(cam) is comparable to that in P-450$_{cam}$(adanone) (Figure 2), whereas P-450$_{cam}$(0) and P-450$_{cam}$(norcam) behave differently. This leads to the possibility that the water molecule that is coordinated in the Fe^{III} forms of class 1 complexes (but expelled in the reduced form) might remain close to the heme pocket and constitute an obstacle to ligand escape. The remarkable achievement of the crystal structure of the unstable oxygenated (O$_2$)Fe^{II}P-450$_{cam}$(cam) species reveals surprising changes in the water occupancy with ligand (*48*). In the presence of oxygen, two additional water molecules, not found in the pentacoordinated or in the carbonylated complex, take part in a water network involving Thr252 and are thought to be involved in the proton shuttle required for catalytic activity. This highlights the great versatility of hydration water as well as the difficulty in predicting its presence and role even upon minor changes in the pocket.

High and Low Enthalpy Subsets of CS in Cytochromes P-450. Conformational substates in cytochromes P-450 are often organized in pairs with different CO rebinding properties giving rise to a bimodal $P(H)$ (*4*). Whereas two CS subsets can be identified systematically in P-450$_{SCC}$ and P-450$_{LM2}$ complexes both in the presence and in the absence of a substrate, the situation is more complicated in P-450$_{cam}$. Here, the observation of subsets is strongly substrate dependent. In this work two subsets were observed in P-450$_{cam}$(cam) while P-450$_{cam}$(0), P-450$_{cam}$(norcam), and P-450$_{cam}$(adanone) showed only one population of CS. We mentioned in the previous sections that the latter complexes might actually also present two subsets that are either degenerate and not resolvable experimentally or that one of the subsets strongly dominates at all temperatures.

The present work adds one more piece of information to the yet unsolved puzzle of the dual CS subsets. As evident in Figure 4c, the camphor$_{l.e.}$ and camphor$_{h.e.}$ subpopulations differ by a global shift of about 6−7 kJ/mol of both H^* and H°. The low enthalpy subpopulation is now identified as an exception that does not fit into the ordering of the activation enthalpies according to substrate encumbrance. To understand the nature of the subpopulations requires gathering data on a larger number of substrates. Work along these lines is currently in progress in our laboratory.

[6] The experimental distributions at 293 K are probably truncated because of the time resolution of our equipment. We use the extrapolated value.

CONCLUSION

Relaxation in Hemoproteins. Relaxation in Mb has long been thought to result from heme doming and iron moving out of the heme plane. Rebinding with the "relaxed heme" was found to be slow, rather comparable to our G^{II} process with an enthalpy distribution shifted by about 11−12 kJ/mol toward high values. This view has been repeatedly questioned by several groups, based on a variety of evidence. Presently, the "blocking water" hypothesis (*38*) remains a possible explanation, though the multiple docking sites model has recently received strong experimental support (*14*, *15*).

In cytochrome P-450$_{cam}$ relaxation achieves qualitatively comparable effects as far as rebinding kinetics are concerned, but the underlying mechanism is of an entirely different nature. In the relaxed and ligand-free conformation P° access to the heme is blocked to a variable extent depending on the substrate. The barrier is high because the substrate is close to the heme normal and exerts a severe steric repulsion for CO binding. In the bound state, substrate and heme have moved with respect to the average protein backbone in order to accommodate the almost perpendicular Fe−CO bond geometry. Kinetic data alone do not permit to decide whether CO binding and substrate motion take place in sequence or concomitantly. In the latter case, the kinetic scheme would directly lead from B° to A* (Scheme 1), without any other consequence than a relabeling of the rate parameters. Photodissociation of the Fe−CO bond has two effects: The heme iron relaxes immediately, and the steric strain exerted by the ligand upon the substrate is suddenly relieved (state P*), triggering the relatively slow relaxation of substrate and heme to their ligand-free positions. A significant fraction of CO molecules rebind quickly in P* before relaxation causes the access to the heme to be closed again. Apparently, water plays no direct role in the relaxation process, but it might possibly interfere with CO escape in some complexes.

In conclusion, except for the initial fast relaxation of the heme iron, there is probably no unique process to explain the relaxation kinetics of different hemoproteins. Even with the same protein, the rate-limiting process might differ with the ligand (CO, O2, ...), in the event that the latter might be undergoing specific interactions with internal water molecules or particular protein residues. Though Mb remains a paradigm for general concepts, such as the existence of a hierarchy of CS, protein dynamics display a variety of situations that can be understood only by investigating more complex systems.

ACKNOWLEDGMENT

We are greatly indebted to Dr. Carmelo Di Primo for the generous gift of cytochrome P-450$_{cam}$ and to Prof. S. Yedgar for critical reading of the manuscript.

REFERENCES

1. Austin, R. H., Beeson, K. W., Eisenstein, L., Frauenfelder, H., and Gunsalus, I. C. (1975) *Biochemistry 14*, 5355−5373.
2. Lavalette, D., and Tetreau, C. (1988) *Eur. J. Biochem. 177*, 97−108.

3. Ehrenstein, D., and Nienhaus, G. U. (1992) *Proc. Natl. Acad. Sci. U.S.A. 89*, 9681−9685.
4. Tetreau, C., Di Primo, C., Lange, R., Tourbez, H., and Lavalette, D. (1997) *Biochemistry 36*, 10262−10275.
5. Tetreau, C., Tourbez, M., Gorren, A., Mayer, B., and Lavalette, D. (1999) *Biochemistry 38*, 7210−7218.
6. Ansari, A., Berendzen, J., Bowne, S. F., Frauenfelder, H., Iben, I. E. T., Sauke, T. B., Shyamsunder, E., and Young, R. D. (1985) *Proc. Natl. Acad. Sci. U.S.A. 82*, 5000−5004.
7. Ansari, A., Berendzen, J., Braunstein, D., Cowen, B. R., Frauenfelder, H., Hong, M. K., Iben, I. E. T., Johnson, J. B., Ormos, P., Sauke, T. B., Scholl, R., Schulte, A., Steinbach, P. J., Vittitow, J., and Young, R. D. (1987) *Biophys. Chem. 26*, 337−355.
8. Berendzen, J., and Braunstein, D. (1990) *Proc. Natl. Acad. Sci. U.S.A. 87*, 1−5.
9. Mourant, J. R., Braunstein, D. P., Chu, K., Fauenfelder, H., Nienhaus, G. U., Ormos, P., and Young, R. D. (1993) *Biophys. J. 65*, 1496−1507.
10. Johnson, J. B., Lamb, D. C., Frauenfelder, H., Müller, J., McMahon, B., Nienhaus, G. U., and Young, R. D. (1996) *Biophys. J. 71*, 1563−1573.
11. Lavalette, D., Tetreau, C., Brochon, J.-C., and Livesey, A. (1991) *Eur. J. Biochem. 196*, 591−598.
12. Agmon, N., and Hopfield, J. J. (1983) *J. Chem. Phys. 79*, 2042−2053.
13. Scott, E. E., and Gibson, Q. H. (1997) *Biochemistry 36*, 11909−11917.
14. Ostermann, A., Waschipky, R., Parak, F. G., and Nienhaus, G. U. (2000) *Nature 404*, 205−208.
15. Chu, K., Vojtchovsky, J., McMahon, B. H., Sweet, R. M., Berendzen, J., and Schlichting, I. (2000) *Nature 403*, 921−923.
16. Steinbach, P. J., Ansari, A., Berendzen, J., Braunstein, D., Chu, K., Cowen, B. R., Ehrenstein, D., Frauenfelder, H., Johnson, J. B., Lamb, D. C., Luck, S., Mourant, J. R., Nienhaus, G. U., Ormos, P., Philipp, R., Xie, A., and Young, R. D. (1991) *Biochemistry 30*, 3988−4001.
17. Nienhaus, G. U., Mourant, J. R., and Frauenfelder, H. (1992) *Proc. Natl. Acad. Sci. U.S.A. 89*, 2902−2906.
18. Lim, M., Jackson, T. A., and Anfinrud, P. A. (1993) *Proc. Natl. Acad. Sci. U.S.A. 90*, 5801−5804.
19. Ansari, A., Jones, C. M., Henry, E. R., Hofrichter, J., and Eaton, W. A. (1994) *Biochemistry 33*, 5128−5145.
20. Kuriyan, J., Wilz, S., Karplus, M., and Petsko, G. A. (1986) *J. Mol. Biol. 192*, 133−154.
21. Quillin, M. L., Arduini, R. M., Olson, J. S., and Phillips, G. N., Jr. (1993) *J. Mol. Biol. 234*, 140−155.
22. Vojtechovsky, J., Chu, K., Berendzen, J., Sweet, R. M., and Schlichting, I. (1999) *Biophys. J. 77*, 2153−2174.
23. Cheng, X., and Schoenborn, B. P. (1991) *J. Mol. Biol. 220*, 381−399.
24. Ösapay, K., Theriault, Y., Wright, P. E., and Case, D. A. (1994) *J. Mol. Biol. 244*, 183−197.
25. Quillin, M. L., Li, T., Olson, J. S., Phillips, G. N., Jr., Dou, Y., Ikeda-Saïto, M., Regan, R., Carlson, M., Gibson, Q. H., Li, H., and Elber, R. (1995) *J. Mol. Biol. 245*, 416−436.
26. Agmon, N. (1988) *Biochemistry 27*, 3507−3511.
27. Srajer, V., and Champion, P. (1991) *Biochemistry 30*, 7390−7402.
28. Agmon, N., and Sastry, G. M. (1996) *Chem. Phys. 212*, 207−219.
29. Ormos, P., Szaraz, S., Cupane, A., and Nienhaus, G. U. (1998) *Proc. Natl. Acad. Sci. U.S.A. 95*, 6762−6767.
30. Franzen, S., Bohn, B., Poyart, C., and Martin, J. L. (1995) *Biochemistry 34*, 1224−1237.
31. Balasubramanian, S., Lambright, D. G., Marden, M. C., and Boxer, S. G. (1993) *Biochemistry 32*, 2202−2212.
32. Lambright, D. G., Balasubramanian, S., and Boxer, S. G. (1993) *Biochemistry 32*, 10116−10124.
33. Franzen, S., and Boxer, S. G. (1997) *J. Biol. Chem. 272*, 9655−9660.
34. Hagen, S. J., Hofrichter, J., and Eaton, W. A. (1995) *Science 269*, 959−962.
35. Hagen, S. J., Hofrichter, J., and Eaton, W. A. (1996) *J. Phys. Chem. 100*, 12008−12021.
36. Post, F., Doster, W., Karvounis, G., and Settles, M. (1993) *Biophys. J. 64*, 1833−1842.
37. Sastri, G. M., and Agmon, N. (1997) *Biochemistry 36*, 7097−7108.
38. Kleinert, T., Doster, W., Leyser, H., Petry, W., Schwarz, V., and Settles, M. (1998) *Biochemistry 37*, 717−733.
39. Unger, B. P., Gunsalus, I. C., and Sligar, S. G. (1986) *J. Biol. Chem. 261*, 1158−1163.
40. Doster, W., Beece, D., Bowne, S. F., DiIorio, E. E., Eisenstein, L., Frauenfelder, H., Reinisch, L., Shymsunder, E., Winterhalter, K. H., and Yue, K. T. (1982) *Biochemistry 21*, 4831−4839.
41. Dlott, D. D., Frauenfelder, H., Langer, P., Roder, H., and DiIorio, E. E. (1983) *Proc. Natl. Acad. Sci. U.S.A. 80*, 6239−6243.
42. Young, R. D., and Bowne, S. F. (1984) *J. Chem. Phys. 81*, 3730−3737.
43. Beece, D., Eisenstein, L., Frauenfelder, H., Good, D., Marden, M. C., Reinisch, L., Reynolds, A. H., Sorensen, L. B., and Yue, K. T. (1980) *Biochemistry 19*, 5147−5157.
44. Schlichting, L., Berendzen, J., Phillips, G. N., Jr., and Sweet, R. M. (1994) *Nature 371*, 808−812.
45. Hartmann, H., Zinser, S., Komninos, P., Schneider, R. T., Nienhaus, G. U., and Parak, F. (1996) *Proc. Natl. Acad. Sci. U.S.A. 93*, 7013−7016.
46. Teng, T.-Y., Srajer, V., and Moffat, K. (1997) *Biochemistry 36*, 12087−12100.
47. Raag, R., and Poulos, T. L. (1989) *Biochemistry 28*, 7586−7592.
48. Schlichting, I., Berendzen, J., Chu, K., Stock, A. M., Maves, S. A., Benson, D. E., Sweet, R. M., Ringe, D., Petsko, G. A., and Sligar, S. G. (2000) *Science 287*, 1615−1622.
49. Poulos, T. L., Finzel, B. C., Gunsalus, I. C., Wagner, G. C., and Kraut, J. (1985) *J. Biol. Chem. 260*, 16122−16130.
50. Poulos, T. L., Finzel, B. C., and Howard, A. J. (1987) *J. Mol. Biol. 195*, 687−700.
51. Helms, V., and Wade, R. C. (1998) *J. Am. Chem. Soc. 120*, 2710−2713.
52. Poulos, T. L., Finzel, B. C., and Howard, A. J. (1986) *Biochemistry 25*, 5314−5322.
53. Di Primo, C., Hui Bon Hoa, G., Douzou, P., and Sligar, S. G. (1990) *Eur. J. Biochem. 193*, 383−386.
54. White, R. E., McCarthy, M.-B., Egeberg, K. D., and Sligar, S. G. (1984) *Arch. Biochem. Biophys. 228*, 493−502.
55. Fisher, M. T., and Sligar, S. G. (1985) *J. Am. Chem. Soc. 107*, 5018−5019.
56. Atkins, W. M., and Sligar, S. G. (1987) *J. Am. Chem. Soc. 109*, 3754−3760.
57. Schulze, H., Hui Bon Hoa, G., and Jung, C. (1997) *Biochim. Biophys. Acta 1338*, 77−92.
58. Jung, C., Schulze, H., and Deprez, E. (1996) *Biochemistry 35*, 15088−15094.
59. Schlichting, I., Jung, C., and Schulze, H. (1997) *FEBS Lett. 415*, 253−257.
60. Raag, R., and Poulos, T. L. (1989) *Biochemistry 28*, 917−922.
61. Raag, R., and Poulos, T. L. (1991) *Biochemistry 30*, 2674−2684.
62. Maillard, P., Schaeffer, C., Tetreau, C., Lavalette, D., Lhoste, J.-M., and Momenteau, M. (1989) *J. Chem. Soc., Perkin Trans. 2*, 1437−1442.
63. Lamb, D. C., Prusakov, V., Engler, N., Ostermann, A., Schellenberg, P., Parak, F. G., and Nienhaus, G. U. (1998) *J. Am. Chem. Soc. 120*, 2981−2982.
64. Tetreau, C., Lavalette, D., Momenteau, M., Fischer, J., and Weiss, R. (1994) *J. Am. Chem. Soc. 116*, 11840−11848.
65. Slebobdnick, C., and Ibers, J. A. (1997) *J. Biol. Inorg. Chem. 2*, 521−525.
66. Lavalette, D., and Tetreau, C. (1990) *Biorheology 27*, 599−604.

BI000920U